Effective parameters for photonic crystals with large dielectric contrast

Ruey-Lin Chern[1,*] and Yu-Tang Chen[2]
[1]*Institute of Applied Mechanics, National Taiwan University, Taipei 106, Taiwan, Republic of China*
[2]*Institute of Photonics and Optoelectronics, National Taiwan University, Taipei 106, Taiwan, Republic of China*
(Received 12 February 2009; revised manuscript received 13 July 2009; published 21 August 2009)

We investigate the effective permittivity ε_e and permeability μ_e for photonic crystals with large dielectric contrast by use of the effective-medium model. In the quasistatic regime, the effective parameters are characterized by the anomalous dispersion near the resonances. For TM polarization, the region of negative ε_e spreads over a wide range of frequency and there exists a frequency interval where ε_e and μ_e are simultaneously negative. For TE polarization, the resonance widths are much smaller and the region of doubly negative parameters is not present. The underlying mechanisms are illustrated with the field patterns associated with the leading and high-order resonances. The effective parameters are also examined by the band structures of the photonic crystal with regard to photonic band gaps and special propagating branches. In the static regime, ε_e and μ_e are simplified to the Maxwell-Garnett mixing rule and the resonance feature becomes insignificant.

DOI: 10.1103/PhysRevB.80.075118 PACS number(s): 42.70.Qs, 41.20.Jb, 78.20.Ci

I. INTRODUCTION

The effective permittivity and permeability are two of the most basic quantities of a composite medium. They are especially important in the study of metamaterials,[1,2] which possess properties not available in naturally occurring materials such as negative permeability[1] and negative index of refraction.[3] These counterintuitive properties come from the interaction of electromagnetic waves with the structure rather than directly from the material composition. In particular, the dielectric photonic structure may exhibit a strong magnetic activity[4] and gives rise to optical properties far from the volume average of the constituent material parameters. This feature is attributed to resonances inside the structure and the fields outweigh the material in characterizing the effective parameters.

To treat a composite structure as in effect a homogeneous medium, the microstructures that compose the medium have to be much smaller than the wavelength λ. The effective parameters are therefore *quasistatic* in nature. In order to determine the effective optical properties of a composite medium, various approaches have been proposed.[5–10] For a periodic microstructure with the lattice period a, the ratio a/λ has to be small for the effective parameters to be valid. The experimental and numerical results show that the negative refraction occurs at $a/\lambda \approx 1/6$ or $1/5$,[3,11] which is indeed not a very small value. A theoretical analysis also confirms the existence of a lower bound of a/λ, above which the negative refraction would occur.[12] Therefore, a suitable effective-medium theory for metamaterials should be able to characterize the effective parameters up to a certain frequency range where the retardation effect and resonance feature are taken into account.[13–17]

A heuristic approach to the problem of effective parameters is to require that the forward scattering of a unit cell of the microstructure, when it is immersed inside the effectively homogeneous background, be zero.[18–23] The respective unit cell is therefore not distinguishable from the surrounding effective medium from the scattering point of view. This approach proves to be useful in obtaining the effective dielectric constant of a composite inhomogeneous medium in the static regime. Similar ideas were further employed for developing approaches to the effective parameters beyond the static regime.[24–26]

In this study, we investigate the effective parameters for photonic crystals made of circular dielectric cylinders. The dielectric contrast is chosen to be large so that a strong magnetic activity may arise.[4,9,27,28] There are some examples of materials with high permittivity. For instance, the dielectric constant of silicon carbide can be 200 at the midinfrared frequency.[27] The ferroelectric ceramic even has the dielectric constant as large as 600 at the microwave frequency.[28] The magnetic activity is attributable to resonance, which is a condition when the fields are enhanced and tend to attain their maximum values. This feature is known as Mie resonance associated with individual dielectric cylinders.[29] In this situation, the cylinder behaves like a dielectric resonator.[30] If the dielectric contrast between the cylinder and surrounding material is sufficiently large, the resonant modes in dielectric resonators possess similar features of those in metal waveguides.[31] In this situation, the resonances associated with the dielectric structure occur at relatively low frequencies (small a/λ) and the effective parameters are therefore applicable. The effective-medium model based on the field averaging over an equivalent unit cell is used to characterize the effective permittivity ε_e and permeability μ_e. In the quasistatic regime, the effective parameters exhibit the Lorentz-type *anomalous* dispersion and give rise to negative values near the resonances. For TM polarization, the electric resonance is the leading-order response and the region of negative ε_e spreads over a wide range of frequency. The magnetic resonance, on the other hand, is a high-order response with a smaller resonance width. In particular, there exists a frequency interval where ε_e and μ_e are simultaneously negative. For TE polarization, the role of electric and magnetic resonances are mutually exchanged and the resonance widths become smaller. The frequency interval of both negative ε_e and μ_e is not present.

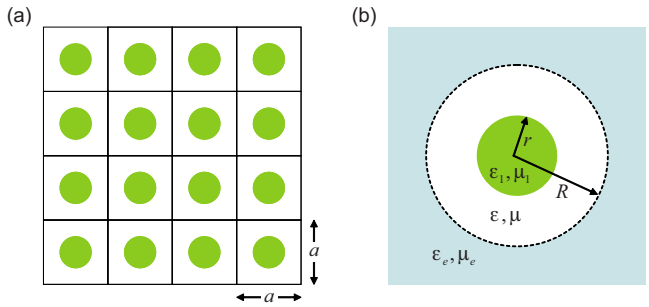

FIG. 1. (Color online) Schematics of (a) the photonic crystal made of circular cylinders and (b) the equivalent unit cell used in the effective-medium model.

The mechanisms of anomalous dispersion for effective parameters are illustrated with the dipole-field patterns at the resonant frequencies. Validity of the effective parameters is further examined by the band structures of the photonic crystal. The regions where either ε_e or μ_e is negative coincide with the photonic band gaps. In the interval where both ε_e and μ_e are negative, there exist two propagating branches with special features. In the static regime, the effective parameters are simplified to the well-known Maxwell-Garnett mixing rule and the resonance feature becomes insignificant.

II. EFFECTIVE-MEDIUM MODEL

A. Effective parameters for TM polarization

Consider a square lattice of dielectric circular cylinders (of radius r) with permittivity ε_1 and permeability μ_1, embedded in the background material with ε and μ. For simplicity, the unit cell (with lattice period a) is approximated by a circular disk having the same area ($\pi R^2 = a^2$). Schematics of the photonic crystal and the equivalent unit cell are plotted in Fig. 1. Let the cylinder axis coincide with the z axis. For TM polarization, where the electric field is oriented along the cylinder axis, the homogenization description of the effective permittivity ε_e and permeability μ_e in terms of average fields is given by

$$\varepsilon_e = \frac{\langle D_z \rangle}{\varepsilon_0 \langle E_z \rangle}, \quad \mu_e = \frac{\langle B_{x,y} \rangle}{\mu_0 \langle H_{x,y} \rangle}, \tag{1}$$

where $\langle \cdot \rangle$ denotes the area averaging (taken over the unit cell) for D_z or $B_{x,y}$ and the line averaging (evaluated at the unit-cell boundary) for E_z or $H_{x,y}$.[1,10] It is assumed that the integration of fields taken on the square unit cell is close to that on the equivalent circular disk. Near the resonance, the electromagnetic fields tend to localize around the cylinders with high permittivity. In this regard, the field distribution within the equivalent unit cell ($0 < \rho < R$) will be close to that for an isolated cylinder. The same approximation has also been used in developing the effective-medium theory and yielding satisfactory results for circular cylinders and spheres.[24,25]

In terms of the cylindrical coordinates (ρ, ϕ) with the origin at the cylinder center, the electric fields are expanded as

$$E_z = \sum_n E_z^{(n)}$$

and $E_z^{(n)} = a_n J_n(k_1 \rho) e^{in\phi}$ for $0 < \rho < r$ and $E_z^{(n)} = [b_n J_n(k\rho) + c_n H_n(k\rho)] e^{in\phi}$ for $r < \rho < R$, where J_n and H_n are the nth-order Bessel and Hankel functions of the first kind, respectively, $k_1 = \sqrt{\varepsilon_1 \mu_1} k_0$, $k = \sqrt{\varepsilon \mu} k_0$, and k_0 is the wavenumber in free space. In the present problem, the Bessel and Hankel functions are elementary solutions to the wave equation in cylindrical coordinates.[32] The Hankel function, however, is singular (the value being infinity) at the cylinder center ($\rho = 0$) and therefore has been excluded from the solution inside the cylinder. The solution outside the cylinder, on the other hand, contains both the Bessel and Hankel functions, which represent the stationary and traveling waves, respectively. The former comes from the incidence and the latter from the scattering by the cylinder. To ensure that the scattered wave is only outgoing at infinity, the radiation condition has to be satisfied. For example, the Sommerfeld radiation condition[33] for a scalar field ϕ (in two dimensions),

$$\lim_{\rho \to \infty} \sqrt{\rho} \left(\frac{\partial}{\partial \rho} - ik \right) \phi = 0,$$

is fulfilled by the Hankel function. Note that $H_n(x) \sim \sqrt{\frac{2}{\pi x}} e^{i(x - n\pi/2 - \pi/4)}$ as $x \to \infty$.[32] The corresponding magnetic fields are obtained by Faraday's law, $(H_\rho, H_\phi) = \frac{i}{\omega \mu} \left(-\frac{1}{\rho} \frac{\partial E_z}{\partial \phi}, \frac{\partial E_z}{\partial \rho} \right)$. Continuity of the tangential electric and magnetic fields (E_z and H_ϕ) at the cylinder surface ($\rho = r$) gives rise to

$$\frac{b_n}{a_n} = \frac{\pi \varepsilon r}{2i} \left[\frac{k}{\varepsilon} J_n(k_1 r) H_n'(kr) - \frac{k_1}{\varepsilon_1} J_n'(k_1 r) H_n(kr) \right], \tag{2}$$

$$\frac{c_n}{a_n} = \frac{\pi \varepsilon r}{2i} \left[\frac{k_1}{\varepsilon_1} J_n'(k_1 r) J_n(kr) - \frac{k}{\varepsilon} J_n(k_1 r) J_n'(kr) \right], \tag{3}$$

where the prime denotes the derivative with respect to the argument.

For TM polarization, the leading-order ($n = 0$) electric fields dominate the electric response. Therefore, $\langle D_z \rangle = 2\pi \varepsilon_0 (\varepsilon_1 \int_0^r E_z^{(0)} \rho d\rho + \varepsilon \int_r^R E_z^{(0)} \rho d\rho) / \pi R^2$ and $\langle E_z \rangle = E_z^{(0)}|_{\rho = R}$ are used in Eq. (1). Using $\int x J_0(x) dx = -x J_0'(x)$, we have

$$\langle D_z \rangle = -\frac{2\varepsilon_0}{R^2} \left\{ \frac{a_0 \varepsilon_1}{k_1} r J_0'(k_1 r) + \frac{b_0 \varepsilon}{k} [R J_0'(kR) - r J_0'(kr)] + \frac{c_0 \varepsilon}{k} [R H_0'(kR) - r H_0'(kr)] \right\}, \tag{4}$$

$$\langle E_z \rangle = b_0 J_0(kR) + c_0 H_0(kR). \tag{5}$$

In the quasistatic regime ($a/\lambda \ll 1$), where the wavelength *outside* the cylinders is much larger than the lattice period, we have $kr \ll 1$ and $kR \ll 1$. Using $J_0(x) \approx 1$, $J_0'(x) \approx -\frac{x}{2}$, $H_0(x) \approx \frac{2i}{\pi} \ln(x)$, and $H_0'(x) \approx \frac{2i}{\pi x}$ as $x \to 0$ in Eqs. (2)–(5), we can obtain $b_0 \approx a_0 J_0(k_1 r)(\varepsilon + \gamma_r \tilde{\varepsilon}_1)/\varepsilon$, $c_0 \approx a_0 J_0(k_1 r)(\varepsilon - \tilde{\varepsilon}_1) \pi k^2 r^2 / 4i\varepsilon$, and

$$\langle D_z \rangle \approx \varepsilon_0 a_0 J_0(k_1 r) [f \tilde{\varepsilon}_1 + (1 - f)(\varepsilon + \gamma_r \tilde{\varepsilon}_1)], \tag{6}$$

$$\langle E_z\rangle \approx a_0 J_0(k_1 r)[(1+f\gamma_R)\varepsilon + (\gamma_r - f\gamma_R)\tilde{\varepsilon}_1]/\varepsilon, \quad (7)$$

where $f=(r/R)^2$ is the fraction of cylinders, $\tilde{\varepsilon}_1=\varepsilon_1\alpha(k_1 r)$, $\gamma_r=\gamma(kr)$, and $\gamma_R=\gamma(kR)$ with

$$\alpha(x) = -\frac{2J_0'(x)}{xJ_0(x)}, \quad \gamma(x) = \frac{x^2}{2}\ln(x), \quad (8)$$

where x stands for $k_1 r$ in $\alpha(x)$ and for kr or kR in $\gamma(x)$. Using Eqs. (6) and (7) in Eq. (1), the effective permittivity is given as

$$\varepsilon_e \approx \varepsilon\frac{(1-f)\varepsilon + [f+(1-f)\gamma_r]\tilde{\varepsilon}_1}{(1+f\gamma_R)\varepsilon + (\gamma_r - f\gamma_R)\tilde{\varepsilon}_1}. \quad (9)$$

In Eq. (8), $\alpha(x)$ is an oscillatory function associated with the circular geometry. Note from Eq. (9) that ε_e diverges as $(1+f\gamma_R)\varepsilon+(\gamma_r-f\gamma_R)\alpha\varepsilon_1\approx 0$ and becomes zero as $(1-f)\varepsilon+[f+(1-f)\gamma_r]\alpha\varepsilon_1\approx 0$. As a result, there exists a region where ε_e is negative. In the static regime ($a/\lambda\approx 0$), where the wavelength *inside* the cylinders is also much larger than the lattice period, we have further $k_1 r \ll 1$. It follows that $\alpha(k_1 r)\approx 1$, $\tilde{\varepsilon}_1\approx\varepsilon_1$, $\gamma_r\tilde{\varepsilon}_1\approx 0$, and $\gamma_R\tilde{\varepsilon}_1\approx 0$. Equation (9) is then simplified to the well-known Maxwell-Garnett mixing rule[34]

$$\varepsilon_e = (1-f)\varepsilon + f\varepsilon_1. \quad (10)$$

In this situation, the effective permittivity is independent of the frequency and the resonance feature becomes insignificant. On the other hand, the first-order ($n=1$) magnetic fields are responsible for the magnetic response. Therefore, $\langle B_x\rangle = \mu_0(\mu_1\int_0^{2\pi}\int_0^r H_x^{(1)}\rho d\rho d\phi + \mu\int_0^{2\pi}\int_r^R H_x^{(1)}\rho d\rho d\phi)/\pi R^2$ and $\langle H_x\rangle = H_x^{(1)}|_{\rho=R,\phi=\pm\pi/2}$ are used in Eq. (1), where

$$H_x^{(1)} = H_\rho^{(1)}\cos\phi - H_\phi^{(1)}\sin\phi$$

Using $\int[J_1(x)+xJ_1'(x)]dx = xJ_1(x)$, we have

$$\langle B_x\rangle = \frac{\mu_0}{\omega R^2}\{a_1 rJ_1(k_1 r) + b_1[RJ_1(kR) - rJ_1(kr)] + c_1[RH_1(kR) - rH_1(kr)]\}, \quad (11)$$

$$\langle H_x\rangle = \frac{k}{\omega\mu}[b_1 J_1'(k\rho) + c_1 H_1'(k\rho)]. \quad (12)$$

In the quasistatic regime, where $kr\ll 1$ and $kR\ll 1$, we use $J_1(x)\approx\frac{x}{2}$, $J_1'(x)\approx\frac{1}{2}$, $H_1(x)\approx -\frac{2i}{\pi x}$, and $H_1'(x)\approx\frac{2i}{\pi x^2}$ as $x\to 0$ in Eqs. (2), (3), (11), and (12) to give $b_1\approx a_1 J_1'(k_1 r)(\mu+\tilde{\mu}_1)k_1/k\mu_1$, $c_1\approx a_1 J_1'(k_1 r)(\mu-\tilde{\mu}_1)\pi r^2 k_1 k/4i\mu_1$, and

$$\langle B_x\rangle \approx \frac{\mu_0 k_1}{2\omega\mu_1}a_1 J_1'(k_1 r)[(1-f)\mu + (1+f)\tilde{\mu}_1], \quad (13)$$

$$\langle H_x\rangle \approx \frac{k_1}{2\omega\mu_1}a_1 J_1'(k_1 r)[(1+f)\mu + (1-f)\tilde{\mu}_1]/\mu, \quad (14)$$

where $\tilde{\mu}_1=\mu_1\beta(k_1 r)$ with

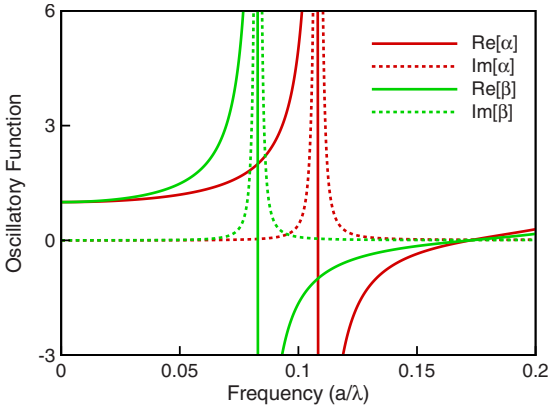

FIG. 2. (Color online) Variations in the oscillatory functions $\alpha(k_1 r)$ and $\beta(k_1 r)$ with the frequency a/λ, where $r/a=0.25$, $\varepsilon_1=200+3i$, $\mu_1=1$, $\varepsilon=1$, and $\mu=1$.

$$\beta(x) = \frac{J_1(x)}{xJ_1'(x)}, \quad (15)$$

where x stands for $k_1 r$. Using Eqs. (13) and (14) in Eq. (1), the effective permeability is given as

$$\mu_e \approx \mu\frac{(1-f)\mu + (1+f)\tilde{\mu}_1}{(1+f)\mu + (1-f)\tilde{\mu}_1}. \quad (16)$$

In Eq. (15), $\beta(x)$ is another oscillatory function associated with the circular geometry. Note from Eq. (16) that μ_e diverges as $\beta\approx -(\frac{1+f}{1-f})\frac{\mu}{\mu_1}$ and becomes zero as $\beta\approx -(\frac{1-f}{1+f})\frac{\mu}{\mu_1}$. For a small fraction f, the region of negative μ_e will be small as well. In the static regime, where $k_1 r\ll 1$, we have $\beta(k_1 r)\approx 1$ and $\tilde{\mu}_1\approx\mu_1$. Equation (16) is then simplified to the well-known Maxwell-Garnett mixing rule[34]

$$\mu_e \approx \mu\frac{(1-f)\mu + (1+f)\mu_1}{(1+f)\mu + (1-f)\mu_1}. \quad (17)$$

A similar procedure of using $\langle B_y\rangle$ and $\langle H_y\rangle$ in Eq. (1) leads to the same expressions of Eqs. (16) and (17). For illustration, the variations in oscillatory functions $\alpha(k_1 r)$ [in Eq. (8)] and $\beta(k_1 r)$ [in Eq. (15)] with the frequency $a/\lambda = ka/2\pi$ are plotted in Fig. 2, where $r/a=0.25$, $\varepsilon_1=200+3i$, $\mu_1=1$, $\varepsilon=1$, and $\mu=1$. Here, ε_1 is much larger than ε and therefore $k_1 r = \sqrt{\varepsilon_1\mu_1}kr$ is not negligible even when kr is small (in the quasistatic regime). The parameter $\varepsilon_1=200+3i$ is chosen to be within a feasible range, the imaginary part being kept at a small number to account for a low loss in the dielectric material. A likewise dielectric parameter has been used in the study of mesoscopic magnetism in the dielectric metamaterial.[35] In the limit as a/λ goes to zero, both α and β approach unity (which can be seen from the asymptotic relations of Bessel functions). This condition is known as the static regime. As a/λ approaches the resonance, where α or β has a *pole* (the denominator being zero), the function grows rapidly to a very large positive value and then drops quickly to a very negative one. As a/λ increases further, α or β returns to positive values after passing a *zero* (where the numerator vanishes). Therefore, there may exist a region where the effective parameter is negative.

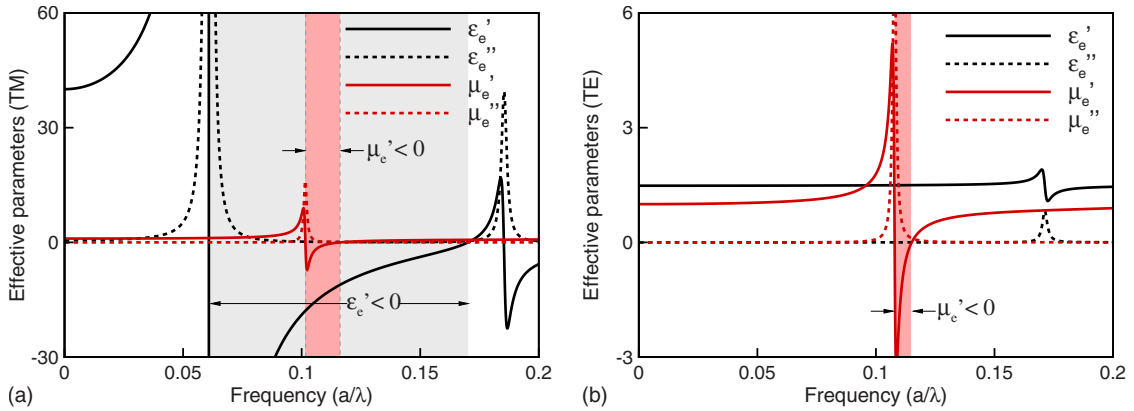

FIG. 3. (Color online) Effective permittivity $\varepsilon_e=\varepsilon_e'+i\varepsilon_e''$ and permeability $\mu_e=\mu_e'+i\mu_e''$ for the photonic crystal of dielectric circular cylinders with $r/a=0.25$, $\varepsilon_1=200+3i$, and $\mu_1=1$ embedded in the background with $\varepsilon=1$ and $\mu=1$ for (a) TM polarization and (b) TE polarization. The shaded areas correspond to the regions for $\varepsilon_e'<0$ or $\mu_e'<0$.

The range of validity of the approximation in the present problem is the region where the resonance dominates the dispersion characteristics. This range corresponds to the frequency band gap and the validity will be confirmed by the band-structure calculation in Sec. III C. Beyond the major resonances, the effective-medium description gradually loses its validity. On the one hand, a larger a/λ indicates that the medium can no longer be considered homogeneous. On the other hand, the presence of high-order modes renders the effective parameters invalid.[36,37]

B. Effective parameters for TE polarization

For TE polarization, where the magnetic field is oriented along the cylinder axis, the homogenization description of the effective parameters is given as

$$\mu_e=\frac{\langle B_z\rangle}{\mu_0\langle H_z\rangle},\quad \mu_e=\frac{\langle D_{x,y}\rangle}{\varepsilon_0\langle E_{x,y}\rangle}. \tag{18}$$

In this polarization, the leading-order ($n=0$) magnetic fields dominate the magnetic response and the first-order ($n=1$) electric fields are responsible for the electric response. The effective parameters can be determined in a similar manner as that for TM polarization. In the quasistatic regime, where $kr\ll 1$ and $kR\ll 1$, we have

$$\mu_e\approx\mu\frac{(1-f)\mu+[f+(1-f)\gamma_r]\tilde{\mu}_1}{(1+f\gamma_R)\mu+(\gamma_r-f\gamma_R)\tilde{\mu}_1},$$

$$\varepsilon_e\approx\varepsilon\frac{(1-f)\varepsilon+(1+f)\tilde{\varepsilon}_1}{(1+f)\varepsilon+(1-f)\tilde{\varepsilon}_1}, \tag{19}$$

where $\tilde{\mu}_1=\mu_1\alpha(k_1r)$ and $\tilde{\varepsilon}_1=\varepsilon_1\beta(k_1r)$. Here, $\alpha(x)$ is responsible for the leading-order magnetic resonance. Note from Eq. (19) that μ_e diverges as $(1+f\gamma_R)\mu+(\gamma_r-f\gamma_R)\alpha\mu_1\approx 0$. For nonmagnetic materials ($\mu_1=\mu=1$), this condition occurs when α goes to infinity (since $\gamma_r-f\gamma_R\approx 0$) or, equivalently, $J_0(k_1r)\approx 0$ [cf. Eq. (8)]. The latter is identified as the condition of TM_{01} mode for circular waveguides.[31] Meanwhile, μ_e becomes zero as $(1-f)\mu+[f+(1-f)\gamma_r]\alpha\mu_1\approx 0$ and there exists a region for $\mu_e<0$. On the other hand, $\beta(x)$ is responsible for the high-order electric resonance. Note also from Eq. (19) that ε_e diverges as $\beta\approx-(\frac{1+f}{1-f})\frac{\varepsilon}{\varepsilon_1}$ and becomes zero as $\beta\approx-(\frac{1-f}{1+f})\frac{\varepsilon}{\varepsilon_1}$. As $\varepsilon_1\gg\varepsilon$ in the present configuration, the region of negative ε_e is close to the frequency for $\beta\approx 0$ and the resonance width will be small. In the static regime, where $k_1r\ll 1$, Eq. (19) is simplified to the Maxwell-Garnett mixing rule[34]

$$\mu_e\approx(1-f)\mu+f\mu_1,\quad \varepsilon_e\approx\varepsilon\frac{(1-f)\varepsilon+(1+f)\varepsilon_1}{(1+f)\varepsilon+(1-f)\varepsilon_1}, \tag{20}$$

It is noted that $\mu_e(\varepsilon_e)$ for TM polarization has exactly the same expression of $\varepsilon_e(\mu_e)$ for TE polarization. This is a consequence of symmetry in source-free Maxwell's equations with respect to electric and magnetic properties.

III. RESULTS AND DISCUSSION

A. Effective permittivity and permeability

Figure 3(a) shows the calculated results of the effective permittivity $\varepsilon_e=\varepsilon_e'+i\varepsilon_e''$ and permeability $\mu_e=\mu_e'+i\mu_e''$ based on Eqs. (9) and (16) for the photonic crystal of dielectric circular cylinders with $r/a=0.25(f\approx 0.196)$, $\varepsilon_1=200+3i$, and $\mu_1=1$ embedded in the background with $\varepsilon=1$ and $\mu=1$ for TM polarization. The effective parameters exhibit the Lorentz-type anomalous dispersion in the vicinities of the leading and high-order resonances, where ε_e' and μ_e' rise abruptly and drop sharply at $a/\lambda\approx 0.061$ and 0.102, respectively. Meanwhile, ε_e'' and μ_e'' attain their maximums at the corresponding resonant frequencies. In particular, the leading-order electric resonance spreads over a rather wide range of frequency; the region for $\varepsilon_e'<0$ is located at $0.061<a/\lambda<0.17$. The magnetic resonance, on the other hand, has a smaller resonance width and the region for $\mu_e'<0(0.102<a/\lambda<0.116)$ is completely within the region for $\varepsilon_e'<0$. Therefore, there exists a frequency interval where ε_e' and μ_e' are simultaneously negative. This feature has also been demonstrated in recent experiments.[27,28] An additional electric resonance occurs at a higher frequency $a/\lambda\approx 0.185$

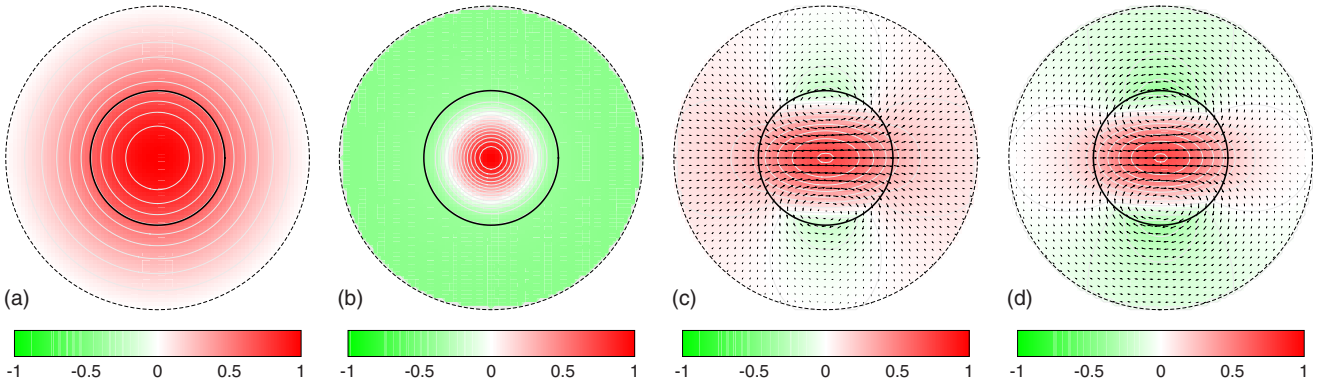

FIG. 4. (Color online) Field contours of $E_z^{(0)}$ at (a) $a/\lambda=0.061$ and (b) 0.17, and field vectors of $(H_x^{(1)},H_y^{(1)})$ at (c) $a/\lambda=0.102$ and (d) 0.116 for the photonic crystal in Fig. 3 for TM polarization. The fields are normalized to have unity maximum magnitude. Red (dark gray) and green (light gray) colors correspond to positive and negative field values, respectively. In (c) and (d), the color represents the value of $H_x^{(1)}$.

but with a smaller resonance width. In the static regime $(a/\lambda\approx 0)$, $\varepsilon_e'\approx 40$, and $\mu_e'\approx 1$, which are consistent with the Maxwell-Garnett mixing rule [cf. Eqs. (10) and (17)].

Figure 3(b) shows the effective parameters for TE polarization based on Eq. (19) for the same photonic crystal. The leading-order magnetic resonance occurs at $a/\lambda\approx 0.108$, which is nearly identical to the cutoff frequency of TM_{01} mode for circular waveguides,[31]

$$\omega_{c_{01}} = x_{01}c/r\sqrt{\varepsilon_1\mu_1} \approx 0.108(2\pi c/a),$$

where $x_{01}\approx 2.405$ is the first root of $J_0(x)=0$. The region for $\mu_e'<0$ is located at $0.108<a/\lambda<0.115$, which is substantially smaller than the region of leading-order resonance for TM polarization [cf. Fig. 3(a)]. On the other hand, the high-order electric resonance occurs at $a/\lambda\approx 0.171$, with a much smaller resonance width. In the presence of ε_1'', the region for $\varepsilon_e'<0$ does not even exist, although the anomalous dispersion feature is still present. In the static regime $(a/\lambda\approx 0)$, $\varepsilon_e'\approx 1.483$, and $\mu_e'\approx 1$, which are consistent with the Maxwell-Garnett mixing rule [cf. Eq. (20)].

B. Illustrations of the leading and high-order resonances

The origin of anomalous dispersion for effective parameters is attributable to resonances associated with the dielectric structure. Figures 4 and 5 illustrate the features of resonances in terms of field patterns. For TM polarization, the leading-order electric resonance is manifest on the field contours of $E_z^{(0)}$, as shown in Figs. 4(a) and 4(b). Near the resonance, the electric fields tend to concentrate in the dielectric region and give rise to electric dipoles along the cylinder axis. In particular, Fig. 4(a) corresponds to $\varepsilon_e'\approx\pm\infty$ at $a/\lambda\approx 0.061$, where the electric field vanishes at the unit-cell boundary $(E_z^{(0)}|_{\rho=R}\approx 0)$, and Fig. 4(b) corresponds to $\varepsilon_e'\approx 0$ at $a/\lambda\approx 0.17$, where the integral of electric displacements over the unit cell is nearly zero $(\int D_z^{(0)}da\approx 0)$. The above two features are consistent with the homogenization description of the effective permittivity in Eq. (1). The region for $\varepsilon_e'<0$ is located between two extremes: $\langle E_z\rangle\approx 0$ (where $\varepsilon_e'\approx\pm\infty$) and $\langle D_z\rangle\approx 0$ (where $\varepsilon_e'\approx 0$). The former indicates that an infinitesimal electric field is able to produce a nonzero electric response and ε_e' is therefore very large while the latter means a nearly null electric response and ε_e' is approximately zero. In another aspect, the obvious distinction be-

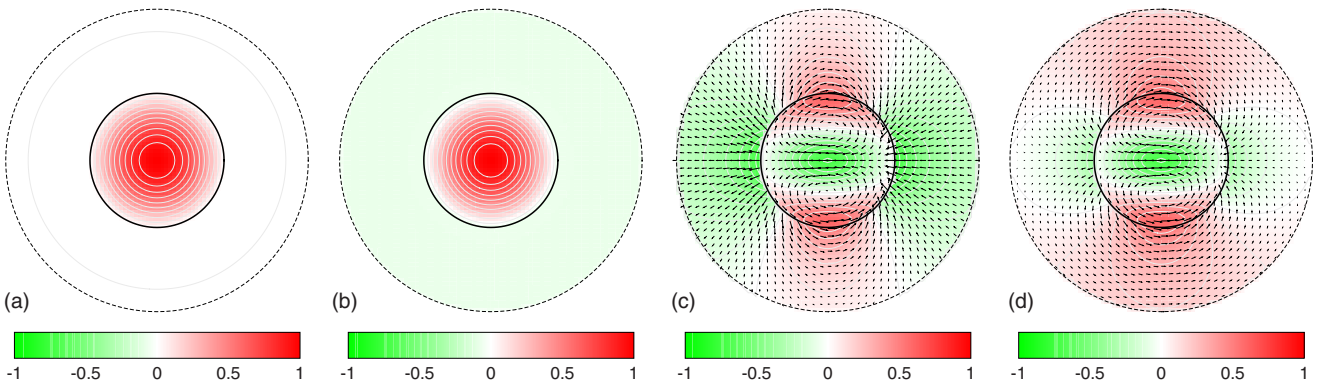

FIG. 5. (Color online) Field contours of $H_z^{(0)}$ at (a) $a/\lambda=0.108$ and (b) 0.115, and field vectors of $(E_x^{(1)},E_y^{(1)})$ at (c) $a/\lambda=0.171$ and (d) 0.172 for the photonic crystal in Fig. 3 for TE polarization. The fields are normalized to have unity maximum magnitude. Red (dark gray) and green (dark gray) colors correspond to positive and negative field values, respectively. In (c) and (d), the color represents the value of $E_x^{(1)}$.

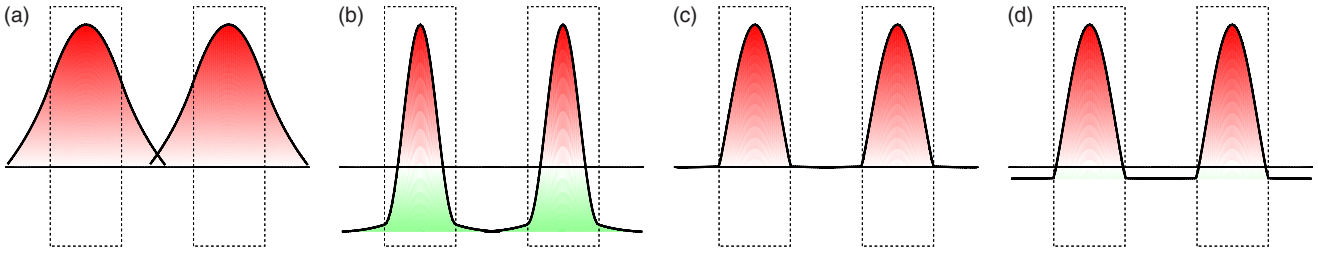

FIG. 6. (Color online) Sectional-field profiles which cover two adjacent cylinders for the resonant field patterns: $E_z^{(0)}$ at (a) $a/\lambda=0.061$ and (b) 0.17 for TM polarization and $H_z^{(0)}$ at (c) $a/\lambda=0.108$ and (d) 0.115 for TE polarization. The dashed lines indicate the locations of cylinders.

tween Figs. 4(a) and 4(b) shows that their resonant frequencies are far different and the region for $\varepsilon_e'<0$ is large [cf. Fig. 3(a)].

On the other hand, the high-order magnetic resonance is manifest on the field vectors of $(H_x^{(1)},H_y^{(1)})$, as shown in Figs. 4(c) and 4(d) for $\mu_e'\approx\pm\infty$ at $a/\lambda\approx0.102$ and $\mu_e'\approx0$ at $a/\lambda\approx0.116$, respectively. Near the resonances, the fields are also concentrated in the dielectric cylinder and the vector distributions depict the magnetic dipoles oriented in the horizontal direction (perpendicular to the direction of electric dipoles). The distinction between Figs. 4(c) and 4(d) is not as significant as that for the electric resonance [cf. Figs. 4(a) and 4(b)] and the region for $\mu_e'<0$ is smaller.

For TE polarization, the leading-order magnetic resonance is manifest on the field contours of $H_z^{(0)}$, as shown in Figs. 5(a) and 5(b). Compared with the electric fields for TM polarization [cf. Figs. 4(a) and 4(b)], the magnetic fields at resonances are much more localized inside the dielectric cylinder, outside which the field intensities are substantially reduced or even become zero. Figure 5(a) corresponds to $\mu_e'\approx\pm\infty$ at $a/\lambda\approx0.108$, where $\langle H_z\rangle\approx0$ ($H_z^{(0)}$ vanishes at the unit-cell boundary), and Fig. 5(b) corresponds to $\mu_e'\approx0$ at $a/\lambda\approx0.115$, where $\langle B_z\rangle\approx0$ (the integral of $B_z^{(0)}$ over the unit cell is zero). Likewise, the above two features are consistent with the homogenization description of the effective permeability in Eq. (1). Note that the field patterns in Figs. 5(a) and 5(b) are alike and the region for $\mu_e'<0$ is small [cf. Fig. 3(b)]. In fact, the field pattern inside the dielectric cylinder resembles TM_{01} mode for circular waveguides,[31] $J_0(x_{01}\rho/r)(x_{01}\approx2.405)$. In another aspect, the high-order electric resonance is manifest on the field vectors of $(E_x^{(1)},E_y^{(1)})$, as shown in Figs. 5(c) and 5(d), where ε_e' experiences a rapid change in the immediate neighborhood of resonance. The field patterns depict the electric dipoles oriented in the horizontal direction, which are similar to those in Figs. 4(c) and 4(d), except that the vector orientations are reversed.

To examine the localization feature of resonant-field patterns, the sectional profiles of Figs. 4(a), 4(b), 5(a), and 5(b) are plotted in Fig. 6. For illustration of the interaction of fields between the cylinders, the field profiles that cover two adjacent cylinders are overlaid in each plot. An estimate of the interaction is given by the overlap area ratio: $R_A\equiv A_{\text{overlap}}/A_{\text{profile}}$, where A_{overlap} is the area of overlap region between two adjacent field profiles, each of which has a sectional area A_{profile}. For TM polarization in Figs. 6(a) and 6(b), the fields are largely confined in the unit cell. The corresponding overlap area ratio is less than 0.5%. For TE polarization in Figs. 6(c) and 6(d), the fields are even localized within the dielectric cylinder and the overlap area ratio is nearly zero.

C. Connection with the band structures

Anomalous dispersion of the effective parameters and the associated resonance features are further examined by the band structures of the photonic crystal. Near the resonances, the fields are localized around individual dielectric cylinders with rather weak interactions between neighboring cells. The propagation of waves inside the structure is therefore hindered. This feature is closely related to the photonic band gaps of the band structures. In the band-gap regions, the resultant wave vectors become purely imaginary and no frequency branches are allowed.[38] This corresponds to the situation where either $\varepsilon_e'<0$ or $\mu_e'<0$. In Fig. 7, the band structures of the corresponding photonic crystal are calculated by the inverse iteration method.[39,40]

Figure 7 shows the band structures for the photonic crystal of dielectric circular cylinders with $r/a=0.25$, $\varepsilon_1=200+3i$, and $\mu_1=1$ embedded in the background with $\varepsilon=1$ and $\mu=1$. The inclusion of imaginary part in the dielectric constant gives rise to complex-frequency branches. The real frequency component has the same meaning as in a lossless system while the imaginary frequency component indicates a decay factor in time and is accountable for the effect of loss. If the imaginary part of the dielectric constant is relatively small, as in the case of present study, the decay factors are also small and the real frequency branches exhibit only a slight discrepancy from those in a lossless system. This feature has been studied for a plasmonic structure which takes into account the effect of damping.[41]

For TM polarization shown in Fig. 7(a), the electric resonance is the leading-order response and gives rise to large photonic band gaps. The first and second gaps ($0.062<a/\lambda<0.1$ and $0.117<a/\lambda<0.169$) basically coincide with the regions where $\varepsilon_e'<0$ and $\mu_e'>0$ [cf. Fig. 3(a)]. In the region between the two gaps, where ε_e' and μ_e' are simultaneously negative, there exist two special propagating branches. The corresponding frequency curves are concave downward in the vicinity of point Γ and the photonic effective mass is considered negative definite.[42] This is also a typical dispersion feature in a negatively refracting material.[43]

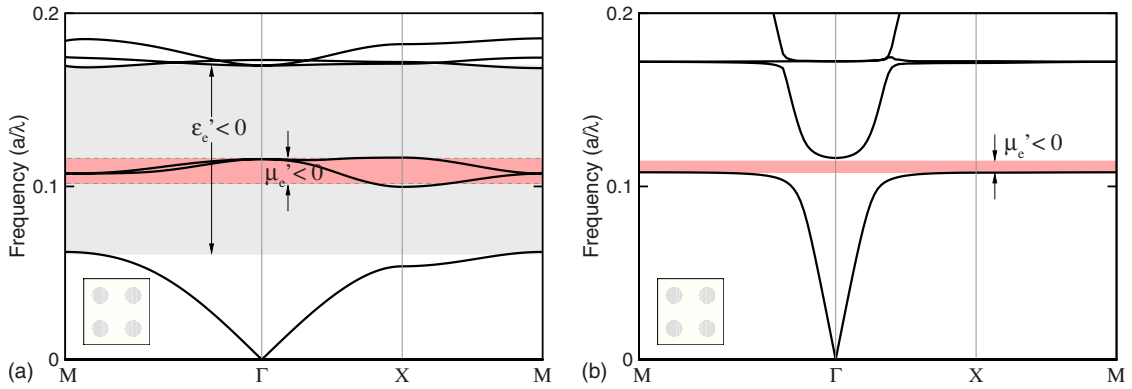

FIG. 7. (Color online) Band structures for the photonic crystal of dielectric circular cylinders with $r/a=0.25$, $\varepsilon_1=200+3i$, and $\mu_1=1$ embedded in the background with $\varepsilon=1$ and $\mu=1$ for (a) TM polarization and (b) TE polarization. The shaded areas correspond to the regions for $\varepsilon_e'<0$ or $\mu_e'<0$ obtained by the effective-medium model [cf. Fig. 3].

The branches lying between the band gaps in Fig. 7(a) are indeed not very flat bands. The respective fields are not purely localized within the cylinder either. This is due to the fact that the tangential electric fields have to be smooth as well as continuous across the dielectric boundary while the magnetic fields are required to be continuous only. As a result, the electric fields are not as localized as the magnetic fields at the high dielectric region. Nevertheless, near the resonance the electric fields are still largely confined within the unit cell, although they may spread out of the cylinder to a certain degree (cf. Fig. 6). The branches between the band gaps, though not very flat, are limited within a small frequency interval ($\Delta\lambda/a\approx0.017$). In this range, ε_e' and μ_e' are simultaneously negative and the region of negative refractive index is therefore not negligible.

For TE polarization shown in Fig. 7(b), the magnetic resonance is the leading-order response and the respective photonic band gap has a much smaller width. Likewise, the gap region ($0.108<a/\lambda<0.116$) basically coincides with the region where $\mu_e'<0$ and $\varepsilon_e'>0$ [cf. Fig. 3(b)]. The frequency branch becomes flattened near the lower band edge, where the resonance frequency is very close to the cutoff frequency of TM_{01} mode for circular waveguides ($a/\lambda\approx0.108$). As the region for $\varepsilon_e'<0$ does not exist, there is no corresponding band gap. Near the electric resonance frequency ($a/\lambda\approx0.172$), the frequency branches become flattened as well.

D. Effective refractive index and figure of merit

Based on the effective permittivity ε_e and permeability μ_e, the effective refractive index n_e can be obtained through the relation: $n_e=\sqrt{\varepsilon_e\mu_e}$. When ε_e and μ_e are treated as complex numbers, $n_e=n_e'+in_e''$ is usually determined by the principal value of square root. Using $n_e=|n_e|e^{i\theta}$, where $|n_e|=\sqrt{(n_e')^2+(n_e'')^2}$ is the complex modulus and $\theta=\tan^{-1}(n_e''/n_e')(-\pi<\theta<\pi)$ is the argument of n_e, one has $|n_e|=\sqrt{|\varepsilon_e||\mu_e|}$ and $\theta=\frac{1}{2}[\tan^{-1}(\varepsilon_e''/\varepsilon_e')+\tan^{-1}(\mu_e''/\mu_e')]$. The real and imaginary parts of n_e are then determined by $n_e'=|n_e|\cos\theta$ and $n_e''=|n_e|\sin\theta$.

Near the resonance, the negative n_e' may be associated with a large n_e'' even in the case of small loss. In order to characterize the quality of negative refractive index, the figure of merit (FOM), defined as $-n_e'/n_e''$, has been proposed.[44] Using ε_e and μ_e for the same structure in Fig. 3, n_e and its FOM are plotted in Fig. 8. It is shown that the region of positive and nonnegligible FOM basically coincides with the range where both ε_e' and μ_e' are negative (denoted by the shaded area). For TM polarization, FOM has its maximum

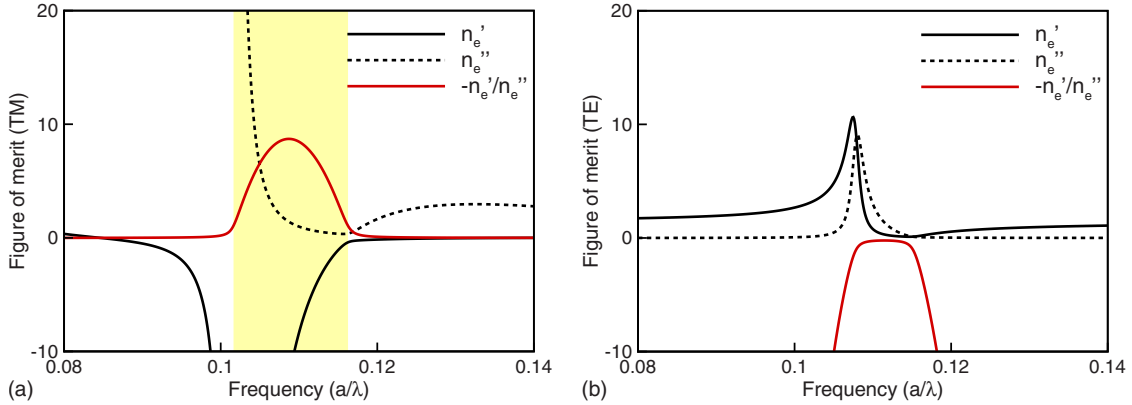

FIG. 8. (Color online) Effective refractive index $n_e=n_e'+in_e''$ and figure of merit $-n_e'/n_e''$ for the same photonic crystal in Fig. 3. (a) TM polarization and (b) TE polarization. The shaded area corresponds to the region where $\varepsilon_e'<0$ and $\mu_e'<0$.

value 8.7 at about the middle point of the double-negative region ($a/\lambda \approx 0.1085$), where $-n_e'$ is large and n_e'' is small. At both edges of the double-negative region, FOM is reduced to a small value and either $-n_e'$ is negligible (the right edge) or n_e'' is very large (the left edge).

Due to the presence of a small loss, the range of negative n_e' is slightly deviated from the double-negative region. There is a small portion (to the left of this region) where $n_e' < 0$ but ε_e' and μ_e' are not simultaneously negative; that is, $\varepsilon_e' < 0$ and $\mu_e' > 0$ [cf. Figure 3(a)]. In this range, n_e'' is quite large and its FOM is negligible. A similar feature has also been observed in the near-infrared negative-index metamaterials.[45] For TE polarization, the corresponding FOM is either negative or negligible. This feature parallels with the fact that there is no frequency range where both ε_e' and μ_e' are negative [cf. Fig. 3(b)].

E. Spatial dispersion and uniaxial anisotropic property

The effective parameters are functions of frequency (a/λ), which means that the temporal dispersion (or the noninstantaneous response) has been considered. A more thorough approach would take into account the spatial dispersion (or the nonlocal effect). Basically, the spatial dispersion increases its importance when the wavelength λ becomes comparable to the characteristic length of the microstructure that composes the medium (e.g., the lattice period a). On the other hand, as the wave number k approaches zero, the spatial dispersion disappears.[46] In the present study, the effective parameters are valid in the quasistatic regime, where a/λ is small (though not negligible). A general description of spatial dispersion appears as a term of k^2.[47,48] This is the case when the medium has the inversion symmetry (nongyrotropic).[49] When the wavelength is relatively long (in the quasistatic regime), the spatial dispersion effect is expected to be small.

In the present problem, the features of effective parameters are mainly characterized by the intrinsic resonances associated with the individual dielectric cylinders (in the form of waveguide resonances). Around the resonant frequencies, the respective fields are localized within the unit cell (for TE polarization, the fields are even localized within the cylinder with relatively weak interactions between the neighboring cells (cf. Fig. 6). In this situation, the nonlocal effect (influences from other unit cells) will be not significant. In particular, the spatial dispersion in periodic structures is attributable to the Bloch scattering by the lattice and its effect on the effective parameter can be described by a multiplication factor: $\sin(\frac{ka}{2})/(\frac{ka}{2})$.[10] At the long wavelength (small ka), this factor would approach unity. For a general situation, however, the effective parameters may depend on the wave number. This effect could be more significant in TM polarization as the respective field patterns are not so localized at the dielectric region as those in TE polarization. In addition, strong spatial dispersion may arise in conducting wire media even in the long wavelength. This occurs when the plasma oscillation is the major resonance mechanism and there is propagation along the wire axis, where k_z is not zero.[50] For nonzero k_z, the spatial dispersion may increase its important to a certain degree. In this situation, decoupled TM and TE modes are no longer available.[51]

In another aspect, the components of effective parameters for TM and TE polarizations indicate a tensor form of the effective parameters. This is a consequence of the uniaxial anisotropic configuration of the problem. For TM polarization, where the electric field is oriented along the cylinder axis, the effective parameters are described by μ_{xx}, μ_{yy}, and ε_{zz}. For TE polarization, where the magnetic field is oriented along the cylinder axis, the effective parameters are described by ε_{xx}, ε_{yy}, and μ_{zz}. The two cases are complementary to each other and combined together to characterize the overall effective properties of the two-dimensional photonic structure.

IV. CONCLUDING REMARKS

In conclusion, the effective parameters for photonic crystals with large dielectric contrast have been investigated. The effective-medium model based on the field averaging over an equivalent unit cell was used to determine the effective permittivity ε_e and permeability μ_e. In the quasistatic regime, the effective parameters are characterized by the Lorentz-type anomalous dispersion in terms of two oscillatory functions associated with the circular geometry. The leading and high-order resonances dominate the basic dispersion characteristics and give rise to the region of negative ε_e or negative μ_e. In particular, there exists a frequency interval where ε_e and μ_e are simultaneously negative for TM polarization. The mechanisms of anomalous dispersion are illustrated with the dipole-field patterns at two extreme conditions, where the effective parameter goes to infinity or becomes zero. These features parallel with the homogenization description of the effective parameters in terms of average fields. The effective parameters also show consistent results with the photonic band gaps and special propagating branches in the band structures of the photonic crystal. In the static regime, the resonance features become insignificant and the effective parameters are simplified to the Maxwell-Garnett mixing rule.

ACKNOWLEDGMENT

This work was supported in part by National Science Council of the Republic of China under Contracts No. NSC 96-2221-E-002-190-MY3 and No. NSC 97-2120-M-002-013.

*chern@iam.ntu.edu.tw

[1] J. B. Pendry, A. J. Holden, D. J. Robbins, and W. J. Stewart, IEEE Trans. Microwave Theory Tech. **47**, 2075 (1999).
[2] D. R. Smith, J. B. Pendry, and M. C. K. Wiltshire, Science **305**, 788 (2004).
[3] R. A. Shelby, D. R. Smith, and S. Schultz, Science **292**, 77 (2001).
[4] S. O'Brien and J. B. Pendry, J. Phys.: Condens. Matter **14**, 4035 (2002).
[5] A. K. Sarychev, R. C. McPhedran, and V. M. Shalaev, Phys. Rev. B **62**, 8531 (2000).
[6] D. R. Smith, S. Schultz, P. Markoš, and C. M. Soukoulis, Phys. Rev. B **65**, 195104 (2002).
[7] C. L. Holloway, E. F. Kuester, J. Baker-Jarvis, and P. Kabos, IEEE Trans. Antennas Propag. **51**, 2596 (2003).
[8] T. Koschny, M. Kafesaki, E. N. Economou, and C. M. Soukoulis, Phys. Rev. Lett. **93**, 107402 (2004).
[9] D. Felbacq and G. Bouchitté, Phys. Rev. Lett. **94**, 183902 (2005).
[10] D. R. Smith and J. B. Pendry, J. Opt. Soc. Am. B **23**, 391 (2006).
[11] R. S. Schechter and S. T. Chun, Appl. Phys. Lett. **91**, 154102 (2007).
[12] I. Tsukerman, J. Opt. Soc. Am. B **25**, 927 (2008).
[13] L. Lewin, Proc. Inst. Electr. Eng. **94**, 65 (1947).
[14] J. E. Sipe and J. V. Kranendonk, Phys. Rev. A **9**, 1806 (1974).
[15] P. C. Waterman and N. E. Pedersen, J. Appl. Phys. **59**, 2609 (1986).
[16] G. D. Mahan, Phys. Rev. B **38**, 9500 (1988).
[17] A. Lagarkov, A. Sarychev, Y. Smychkovich, and A. Vinogradov, J. Electromagn. Waves Appl. **6**, 1159 (1992).
[18] G. B. Smith, J. Phys. D **10**, L39 (1977).
[19] D. Stroud and F. P. Pan, Phys. Rev. B **17**, 1602 (1978).
[20] W. Lamb, D. M. Wood, and N. W. Ashcroft, Phys. Rev. B **21**, 2248 (1980).
[21] G. A. Niklasson, C. G. Granqvist, and O. Hunderi, Appl. Opt. **20**, 26 (1981).
[22] P. Chýlek and V. Srivastava, Phys. Rev. B **27**, 5098 (1983).
[23] R. Luo, Appl. Opt. **36**, 8153 (1997).
[24] Y. Wu, J. Li, Z. Q. Zhang, and C. T. Chan, Phys. Rev. B **74**, 085111 (2006).
[25] X. Hu, C. T. Chan, J. Zi, M. Li, and K. M. Ho, Phys. Rev. Lett. **96**, 223901 (2006).
[26] S. T. Chui and Z. Lin, Phys. Rev. E **78**, 065601(R) (2008).
[27] J. A. Schuller, R. Zia, T. Taubner, and M. L. Brongersma, Phys. Rev. Lett. **99**, 107401 (2007).
[28] L. Peng, L. Ran, H. Chen, H. Zhang, J. A. Kong, and T. M. Grzegorczyk, Phys. Rev. Lett. **98**, 157403 (2007).
[29] C. F. Bohren and D. R. Huffman, *Absorption and Scattering of Light by Small Particles* (Wiley, New York, 1983).
[30] D. Kajfez and P. Guillon, *Dielectric Resonators*, 2nd ed. (Noble, Atlanta, 1998).
[31] D. M. Pozar, *Microwave Engineering*, 3rd ed. (Wiley, New York, 2005).
[32] J. A. Kong, *Electromagnetic Wave Theory* (EMW, Cambridge, 2005).
[33] A. Sommerfeld, *Partial Differential Equations in Physics*, 2nd ed. (Academic, New York, 1949).
[34] J. C. Maxwell-Garnett, Philos. Trans. R. Soc. London, Ser. A **203**, 385 (1904).
[35] N. A. Mortensen, S. Xiao, and D. Felbacq, J. Eur. Opt. Soc. Rapid Publ. **1**, 06019 (2006).
[36] W. Śmigaj and B. Gralak, Phys. Rev. B **77**, 235445 (2008).
[37] C. Rockstuhl, T. Paul, F. Lederer, T. Pertsch, T. Zentgraf, T. P. Meyrath, and H. Giessen, Phys. Rev. B **77**, 035126 (2008).
[38] J. D. Joannopoulos, R. D. Meade, and J. N. Winn, *Photonic Crystals: Molding the Flow of Light*, 2nd ed. (Princeton University Press, Princeton, 2008).
[39] R. L. Chern, C. C. Chang, C. C. Chang, and R. R. Hwang, Phys. Rev. E **68**, 026704 (2003).
[40] R. L. Chern and S. D. Chao, Opt. Express **16**, 16600 (2008).
[41] R. L. Chern, Phys. Rev. E **79**, 017701 (2009).
[42] C. Luo, S. G. Johnson, J. D. Joannopoulos, and J. B. Pendry, Phys. Rev. B **65**, 201104(R) (2002).
[43] J. B. Pendry, Science **306**, 1353 (2004).
[44] S. Zhang, W. Fan, N. C. Panoiu, K. J. Malloy, R. M. Osgood, and S. R. J. Brueck, Opt. Express **14**, 6778 (2006).
[45] S. Zhang, W. Fan, N. C. Panoiu, K. J. Malloy, R. M. Osgood, and S. R. J. Brueck, Phys. Rev. Lett. **95**, 137404 (2005).
[46] L. D. Landau, E. M. Lifshitz, and L. P. Pitaevskii, *Electrodynamics of Continuous Media*, 2nd ed. (Elsevier, Amsterdam, 1984).
[47] J. J. Hopfield, Phys. Rev. **132**, 563 (1963).
[48] M. A. Shapiro, G. Shvets, J. R. Sirigiri, and R. J. Temkin, Opt. Lett. **31**, 2051 (2006).
[49] V. M. Agranovich and Y. N. Gartstein, Phys. Usp. **49**, 1029 (2006).
[50] P. A. Belov, R. Marqués, S. I. Maslovski, I. S. Nefedov, M. Silveirinha, C. R. Simovski, and S. A. Tretyakov, Phys. Rev. B **67**, 113103 (2003).
[51] J. A. Stratton, *Electromagnetic Theory* (McGraw-Hill, New York, 1941).